water

MDPI

Article

Plunging Circular Jets: Experimental Characterization of Dynamic Pressures Near the Stagnation Zone

Grégoire Jamet [1,*], António Muralha [2,3,*], José F. Melo [2], Pedro A. Manso [1] and Giovanni De Cesare [1]

[1] Platform of Hydraulic Constructions (PL-LCH), Civil Engineering Department, Ecole Polytechnique Fédérale de Lausanne (EPFL), 1015 Lausanne, Switzerland; pedro.manso@epfl.ch (P.A.M.); giovanni.decesare@epfl.ch (G.D.C.)
[2] Hydraulics and Environment Department, Laboratório Nacional de Engenharia Civil (LNEC), 1700-075 Lisboa, Portugal; jfmelo@lnec.pt
[3] Civil Engineering, Architecture and Georesources Department-CERIS, Instituto Superior Técnico (IST), Universidade de Lisboa, 1049-001 Lisboa, Portugal
* Correspondence: gregoire.jamet@alumni.epfl.ch (G.J.); amuralha@lnec.pt (A.M.)

Abstract: Spillways are a requirement for dams' safety, mainly preventing overtopping during floods. A common spillway solution involves plunging jets, which dissipate a considerable flow energy in the plunge pool. Energy dissipation has to occur in a controlled manner to avoid endangering the dam foundation and river slopes. Indeed, a scouring process in the downstream riverbed will inevitably develop until equilibrium is reached, otherwise a suitable pre-excavated or concrete lined plunge pool has to be provided. This paper focuses on experimental studies in which particular attention was paid to the dynamic pressures in the plunge pool floor at the vicinity of the jet stagnation zone sampled at 2.4 kHz. A rectangular experimental facility, 4.00 m long and 2.65 m wide, was used as plunge pool. Tests involved a vertical circular plunging jet with velocity ranging from 5 to 18 m/s and plunge pool depth ranging from 4.2 to 12.5 jet diameters. Differences in dynamic pressure measurements are highlighted between transducers located in the inner and outer regions of the jet diameter footprint. Several parameters characterizing the dynamic pressures evidence trends tied with the jet velocity that, to the authors' knowledge, were not dealt in previous research. These can derive from the coupling effects of consequent recirculating motions and air entrainment in the limited-size plunge pool. Both effects, increasing with velocity, cause an reduction in the efficiency of the diffusing jet shear layer. This aspect deserves further investigation to achieve a better understanding and more complete characterization.

Keywords: spillway; plunging jet; experimental research; dynamic pressures; stagnation zone; energy dissipation; scour

Citation: Jamet, G.; Muralha, A.; Melo, J.F.; Manso, P.A.; De Cesare, G. Plunging Circular Jets: Experimental Characterization of Dynamic Pressures Near the Stagnation Zone. *Water* **2022**, *14*, 173. https://doi.org/10.3390/w14020173

Academic Editor: Giuseppe Pezzinga

Received: 22 November 2021
Accepted: 29 December 2021
Published: 9 January 2022

1. Introduction

Scour due to high-velocity jets has been a phenomenon of considerable interest for engineers and researchers since the beginning of the 20th century, during which a major increase was observed in dams' height. The involved phenomena engage in three-phase complex interactions (gas–liquid–solid), and thus require collaboration between many fields of applied science, such as hydraulics and geomechanics, i.e., multiphase fluid mechanics expertise area (ICOLD 2016 [1]).

Since 1998, a series of research projects have been conducted at the Ecole Polytechnique Fédérale de Lausanne (EPFL) on rock scour and especially on near-prototype velocity circular jets of up to 30 m/s (Bollaert [2], Manso [3], Federspiel [4], Duarte [5]). This pioneer project aimed to assess pressure fluctuations in joints, the influence of scour hole geometry, 3D rock mass response and the influence of air entrainement. Scale effects, though they are not eliminated, are kept as small as possible by using near-prototype velocities. Chanson et al. [6] studied scale effects in vertical circular plunging jets, but only with small velocities of up to 4.4 m/s. The desintegration of jets in air due to instabilities

and turbulent fluctuations, creating two-phases flows, was studied by several authors, e.g., Chanson [7], Toombes and Chanson [8], Pfister and Schwindt [9], Carrillo et al. [10]. Guyot et al. [11] studied air entrainment by large-scale plunging jets of up to 10 m fall and assessed that the difficulty predicting air entrainment is due to the huge variety of flow structures in free-falling jets. Other researchers interested in the field experimentally and, more recently, numerically investigated plunging and submerged jets to assess water flow characteristics, diffusion after impact with water and, thus, mean and fluctuating pressures acting on the pool's bottom, e.g., Ervine & Falvey [12], Franzetti & Tanda [13], May & Willoughby [14], Ervine et al. [15], Melo [16], Castillo et al. [17], Castillo & Carrillo [18]. The experimental results in the literature regarding dynamic pressures showed, among other aspects, that mean pressures start to decrease once the diffusing jet core ceases to persist. This phenomenon was observed for pool depth ratios Y/D between 4.0 and 7.5, depending on authors and facility set-ups. Fluctuating pressures increase until a certain pool depth is reached, and then decrease between Y/D = 4.0 and 12.0 depending on the authors (Bollaert & Schleiss [19]; Castillo et al. [17]). In the two previously cited articles, comparing the previous authors' data, not much information was provided regarding the relative location of the sensors compared with the jet's geometric characteristic, in a circular case, the diameter D.

The intersection of the jet centreline with the pool bottom is called the stagnation point. This is where the mean pressures reach a maximum value, the vertical flow velocity is zero and the fluctuations start to build up. That is why a study near the stagnation zone, inside and outside the jet diameter footprint, is hereinafter presented. Manso et al. [20] dealt with a similar approach and studied up to the 4th statistical moment of pressure distributions in this zone. Herein, the 1st and 2nd statistical moments are covered, which present acceptable agreement with results from the literature and are seen as the most relevant from the engineering perspective. Further research is still required regarding the higher-order statistical moments; therefore, they are not presented in this paper.

The present experimental study involves turbulent high-velocity circular jets, and allows for an exploration of the spatial distribution of dynamic pressures on a flat plunge pool bottom in terms of mean dynamic and fluctuating pressures, as well as power spectra recorded at a higher frequency than in the previous cited works. The pressure transducers were placed horizontally at a distance of r from the jet stagnation point. The results of this study showed an important decrease in the mean dynamic pressure between the sensor at $r/D = 0.00$ and sensors at $r/D = 0.25$ to 0.69, an important change in terms of mean, fluctuating pressures and spectra between sensors inside the jet diameter footprint $r/D < 0.50$ and outside $r/D > 0.50$. Additionally, an observation was made regarding the influence of velocity on the results, which could be explained by the recirculating flow currents and a reduction in the shear stress dissipation of the jet due to the higher air concentration in the pool. Under these circumstances, and using a similar method as shown in Manso [3], a non-dimensional Froude number Fr_{pool}, considering the pool width W_{pool} and the jet velocity at issuance V, was implemented to take the pool size influence into account: $Fr_{pool} = V/\sqrt{g \cdot W_{pool}}$.

2. Materials and Methods

2.1. Experimental Arrangement and Test Program

A rectangular experimental facility built at the Laboratório Nacional de Engenharia Civil (LNEC, Lisbon) with a length of 4.00 m and 2.65 m of width is able to produce circular water jets with a maximum velocity at issuance V of 18.0 m/s. The jet nozzle diameter D is 0.072 m, and the water pool depth, Y, can vary from 0.3 to 0.9 m, which corresponds to a pool depth ratio Y/D ranging from 4.2 to 12.5. The nozzle exit is located 1.0 m above the facility bottom, where the pressure transducers are installed on a metallic plate. Two photographs of the facility are presented in Figure 1.

Five sensors *Kulite XTM-190 (M)—17 Bar* were placed. The full scale output (FSO) is 75 mV for a 17 Bar pressure range with an accuracy of 1% of the FSO due to non-linearity

and hysteresis. The diameter of the transducer sensitive area is 3.8 mm. An excitation is needed for these sensors but only up to 10–12 V, which was provided by an HBM "Spider 8" data acquisition system. Preliminary tests considering acquisition frequencies of up to 9.6 kHz could establish the sampling rate of 2.4 kHz as the lowest one that captures the whole turbulent energy content. If a too low acquisition frequency was used, information about the energy distribution in spectral representations could be lost, especially for higher jet velocities. Thus, the considered acquisition frequency was 2.4 kHz, with a sampling duration of 218 s, to obtain 2^{19} = 524,288 samples per transducer.

The sensors were placed at different radial distances r from the jet centreline (or stagnation point), as represented in Figure 2. One sensor was placed at the jet centreline $r/D = 0.00$ and three others inside the jet diameter footprint ($r/D < 0.5$) at $r/D = 0.25$ and 0.35. Finally, one sensor was located out of the jet diameter footprint at $r/D = 0.69$. Compared to the literature, these sensors' location allowed a refined pressure study near the stagnation zone. Having two sensors at $r/D = 0.35$ allowed to validate the symmetry of the facility in terms of pressure field by checking the average, standard deviation, weight of extreme pressures with Skewness and Kurtosis parameters.

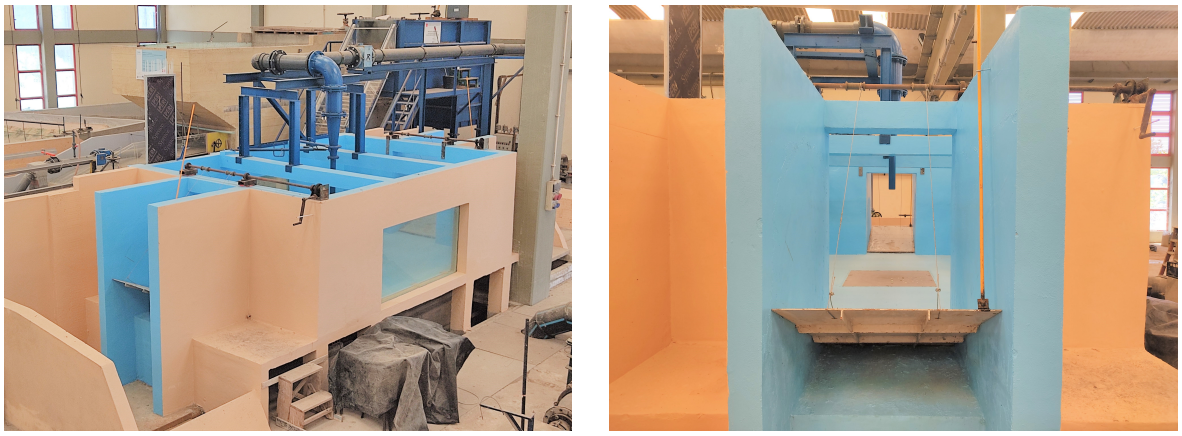

(**a**) (**b**)

Figure 1. Photographs of the experimental facility at LNEC, Lisbon: (**a**) General view, (**b**) View from a flapgate.

Following Bollaert & Schleiss [21] and Manso et al. [22], the kinetic energy correction factor ϕ was observed to be $\phi \approx 1$–1.1. In the present study, the raw values of mean dynamic coefficient Cp showed values higher than $Cp = 1$ (see definition of Cp in the next section). As a result, it was decided to fix the maximum value at $Cp = 1$ and infer the associated correction factor ϕ. Those values are dependent on velocities and range from 1 to 1.096, confirming what is presented in the literature. The non-dimensional Froude pool number $Fr_{pool} = V/\sqrt{g \cdot W_{pool}}$ was considered for the assessment of the influence of pool dimensions in pressure field as velocity significantly increases. The test program and conditions are presented in Tables 1 and 2 using six different discharges and seven pool depths:

Table 1. Test program varying discharge Q and pool depth Y (42 tests).

Q [l/s]	V [m/s] (Fr_{pool})	Y [m] (Y/D)
20	5.0 (0.98)	0.3 (4.2)
30	7.4 (1.45)	0.4 (5.6)
40	9.8 (1.92)	0.5 (6.9)
49	12.0 (2.35)	0.6 (8.3)
60	14.7 (2.88)	0.7 (9.7)
73	18.0 (3.53)	0.8 (11.1)
		0.9 (12.5)

Table 2. Jet test conditions in terms of velocity at issuance V, at impact V_j, kinetic energy correction factor ϕ, Reynolds Re, Froude Fr, Froude Pool Fr_{pool} numbers and jet break-up length ratio H/L_b.

V [m/s]	V_j [m/s]	ϕ [-]	$Re * 10^5$ [-]	Fr [-]	Fr_{pool} [-]	H/L_b [-]
5.0	5.2–6.2	1.000	3.1	5.9	0.98	0.04–0.68
7.4	7.5–8.3	1.083	4.7	8.8	1.45	0.04–0.59
9.8	9.9–10.5	1.075	6.1	11.7	1.92	0.03–0.54
12.0	12.1–12.6	1.058	7.5	14.3	2.35	0.03–0.50
14.7	14.8–15.2	1.019	9.2	17.5	2.88	0.03–0.46
18.0	18.1–18-4	1.096	11.3	21.4	3.53	0.03–0.43

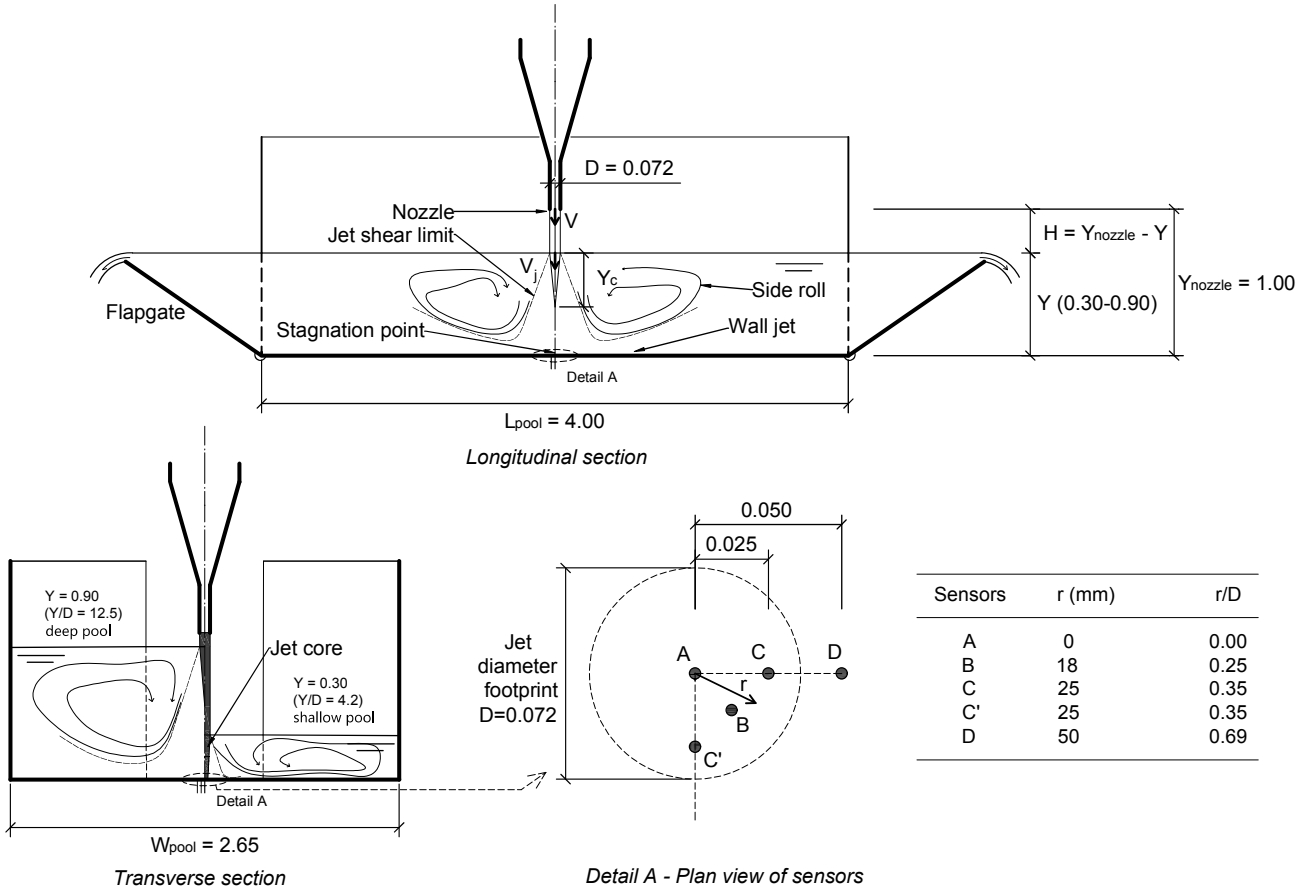

Figure 2. Scheme of the experimental facility—*Dimensions in meters*.

According to visual observation, the jet at V = 5.0 m/s is a smooth turbulent jet. Then, the first important change in the physical properties occurs at around 9.8 m/s, and a second change occurs between 14.7 and 18.0 m/s when the jet becomes unstable and the spreading effect becomes more intense. These observations are similar to those in Ervine and Falvey [12]. As more air is entrained for higher jet velocities, progressive changes are observed in the flow characteristics in the plunge pool (cf. Figure 3).

Turbulence intensity at the jet nozzle issuance was not measured in the present study. Based on other studies, such as that of Manso et al. [20,22], who studied similar jets, at issuance, turbulence intensity Tu was between 4 and 8% for velocities ranging from 10 to 30 m/s. These Tu are more common in ski jump outlet jets than in free overfall jets that have a Tu lower than 3%. Using this assumption for Tu (values between 4 and 8%), one can estimate the range of the jet break-up length H/L_b for each tested jet velocity (cf. Equation (1) and Table 2).

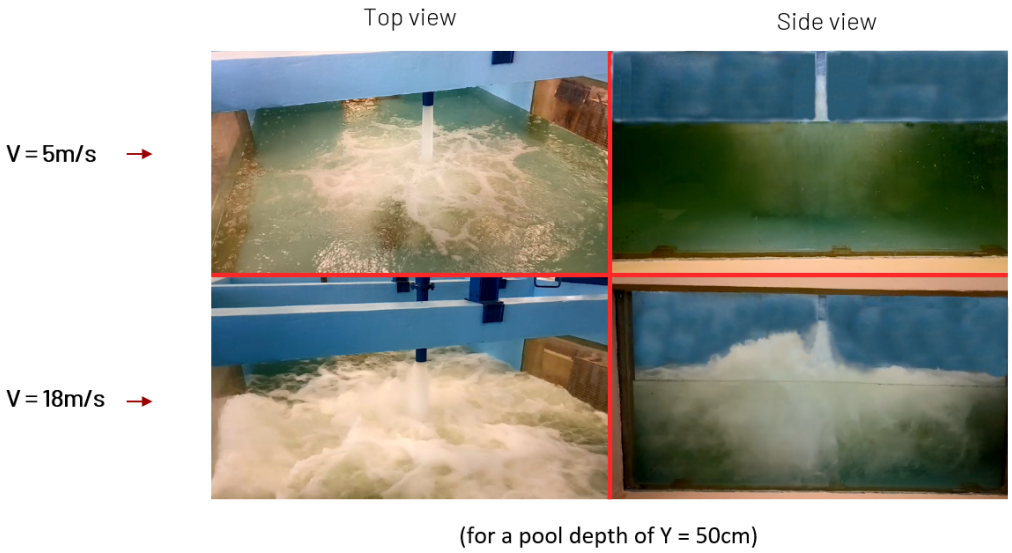

Figure 3. Side and top view of the facility with minimum velocity 5.0 m/s and maximum 18.0 m/s.

Ervine et al. [15], defined the jet break-up length L_b for circular jet based on experimental results as:

$$\frac{L_b}{D \cdot Fr^2} = \frac{1.05}{C^{0.82}} \quad \Rightarrow \quad L_b = \frac{1.05 \cdot D \cdot Fr^2}{C^{0.82}} \tag{1}$$

where Fr is the Froude number, D is the jet diameter at the exit of the nozzle and the parameter C is defined as:

$$C = 1.14 \cdot T_u Fr^2 \tag{2}$$

The minimum value for H/L_b is for a high pool depth and the maximum value is for a low pool depth. Anyhow, given that $H/L_b \leq 0.68$ for all tests, the jet impacting the water is undeveloped. In fact by making the assumption of Tu between 4–8%, the average value H/L_b of all our tests is $H/L_b \approx 0.23$.

2.2. About Scale Effects

The presentation of the experimental arrangement should be accompanied by a discussion on scale effects. Indeed, even if velocity, aeration and spectral content are similar to prototype conditions, the fact that the geometry of the pool and jet are scaled down might lead to scale effects.

To ensure flow similarity between the experimental set-up and specific case studies involving different geometrical and flow values, one has to ensure that the relationship between the flow inertial forces and, respectively, gravity forces (Froude number), flow resistance (Reynolds number), surface tension (Weber number) and turbulence intensity are maintained.

Regarding gravity and resistance forces, these relationships are inherently respected as long as the considered liquid is water and the involved Reynolds number is above 10^5 (negligible influence of viscosity).

Regarding the turbulence intensity, although it was not directly measured in this research, data from similar experimental set-ups, namely those from Manso et al. [20,22], allow to estimate turbulence intensity in the range between 4% and 8%. Melo [16], based on experimental results by Chen & Davis [23], Ervine et al. [24] and Ervine & Falvey [12] infers that, for issuance turbulence intensity of free jets over approximately 3%, the forces associated with either surface tension or viscosity become negligible, the dominant ones being those associated with turbulence intensity. Regarding the conditions for the onset of free surface aeration, Ervine & Falvey [12] estimate that a minimum value of turbulent velocity u'= 0.275 m/s has to be ensured. Considering a turbulence intensity range of 4 to 8%, aeration onset requires mean jet velocities higher than, respectively, $V = u'/Tu$ = 6.9

and 3.4 m/s. With experiments performed over a range from 5 to 18 m/s, the tests were conducted under conditions enabling free surface aeration of the jet at nozzle issuance. Based on the above, it is acceptable to consider that the experiments reproduced prototype spillways under turbulent-free jet aeration conditions.

However, regarding the flow inside the plunge pool, air bubble buoyancy forces and air compressibility play relevant roles regarding the penetration depth of entrained air bubbles, which is linked, among other aspects, to the bubble's rising velocity. Regarding this parameter, Ervine & Falvey [12] estimate the rising velocity of air bubbles at approximately 0.25 m/s; therefore, scale effects in Froude similarity approaches are to be expected. The consideration of a fixed value of a bubble's rising velocity is, however, a simplification of the involved phenomena, as it disregards, among other factors, the compressibility of air in the buoyancy effect, as was pointed out by Melo [25].

In terms of pool geometry, by considering fixed-plan dimensions for a wide range of jet discharges, the side walls influence on the plunge pool flow pattern increases for increasing discharges, i.e., the solid boundaries of the facility have an influence on the obtained results. Another aspect that must be taken into account concerns the wall friction that develops by the wall jet along the pool bottom. A polished brass surface was considered to materialize the pool floor at the deflection zone in order to minimize the influence of the wall friction. No assessment was made, however, of the influence of the pool floor roughness on the plunge pool energy dissipation conditions, with the obtained results being applicable to flat and smooth pool floors (for example, concrete-lined plunge pools).

From the above, it should be outlined that, although the experimental set-up allows for near-prototype flow features regarding velocity, jet aeration, flow resistance and turbulent fluctuations, all of which can be addressed for case study uses based on Froude similarity, one must consider that the results can be affected, to some degree, by plunge pool aeration scale effects and pool plan size (expressed by the width W_{pool}) when transferring results to different size set-ups.

3. Impact Pressures at the Stagnation Zone—Results and Discussion

The following non-dimensional pressure coefficients were considered when characterizing the hydrodynamic actions on the bottom of the pool:

- The mean dynamic pressure coefficient:

$$C_p = \frac{P_{mean} - Y}{\phi \cdot V_j^2/2g} \tag{3}$$

- The fluctuating dynamic pressure coefficient:

$$C'_p = \frac{\sigma}{\phi \cdot V_j^2/2g} \tag{4}$$

where P_{mean} is the time-averaged absolute pressure and $\phi \cdot V_j^2/2g$ the incoming kinetic energy head of the jet (cf. Table 2), $\sigma = \sqrt{\frac{\sum(p_i - P_{mean})^2}{(n-1)}}$ is the standard deviation of the measured pressures. The velocity at impact with water V_j is computed considering the fall length H, following Bernoulli's equation for conservation of energy: $V_j = \sqrt{V^2 + 2g \cdot H}$.

3.1. Radial Study of Mean Dynamic Pressures—$0.00 \leq r/D \leq 0.69$

In Figures 4 and 5, the mean hydrodynamic forces transmitted to the pool floor can be studied in terms of mean dynamic pressure coefficient Cp [-] as a function of pool depth ratio Y/D [-]. Y/D is important to characterize the diffusion length of the jet through the water. This diffusion is closely linked to the jet energy dissipation, which is a key aspect of plunge pool efficiency. Figure 4 is focusing on the stagnation point at $r/D = 0.00$ for each jet velocity, while Figure 5 is a plot of Cp at four radial distances available up to

$r/D = 0.69$ in six graphs, respectively, for each velocity used. Comparisons are made with some previous authors using circular and rectangular jets. For example, Ervine et al., 1997 [15], using a similar circular jet, clearly specified that their data come from the "center transducer location coinciding with the centreline of the jet axis", allowing for a direct comparison with the results of the sensor at $r/D = 0.00$.

By analyzing Cp specifically at the stagnation point $r/D = 0.00$ (cf. Figure 4), it can be mentioned:

(a) **Core persistence (core length Y_c) for r/D = 0.00**: Y_c is defined as the depth required to develop the core jet and the starting depth to observe a decrease in Cp. For the lowest velocities with $Fr_{pool} \leq 1.92$, the core length Y_c did not develop deeper than $8.3D$. For the highest velocities with $Fr_{pool} \geq 1.92$ the core length Y_c did not develop deeper than $9.7D$. The pool depth of $12.5D$ imposed an important decrease in Cp for all tests, except the one with the lowest velocity ($Fr_{pool} = 0.98$). Generally, the core length Y_c was deeper when comparing the Y_c obtained by other authors, as represented in Figure 4. Table 3 summarizes the different core lengths Y_c observed following each jet velocity. By using Table 3, it is possible to define shallow and deep pools. The fundamental question is whether the jet core (with a centreline velocity equal or close to the jet issuance velocity) prevails in depth and impacts the plunge pool bottom. In terms of pressure signature, one can define any pool with stagnation pressures equal or close to $\phi \cdot V_j^2/2g$ as shallow pools. The Limited Depth Diffusion Model (LDDM) compiled and presented in Manso et al. [26] provides an adequate framework.

Table 3. Core persistence (or core length) Y_c depending on jet velocity V.

V [m/s] (Fr_{pool})	Y_c [m]
5.0 (0.98)	<4.2 D
7.4 (1.45)	5.6 D
9.8 (1.92)	8.3 D
12.0 (2.35)	8.3 D
14.7 (2.88)	9.7 D
18.0 (3.53)	9.7 D

A shallow pool depth Y is thus considered for a given velocity when the core jet impacts the pool bottom ($Y < Y_c$). A deep pool depth Y is considered for a given velocity when the core jet is already diffused and, thus, a developed jet is impacting the pool bottom ($Y > Y_c$). A schematic representation is available on the transverse section of Figure 2.

(b) **Maximum mean dynamic pressure for r/D = 0.00**: Increase up to the maximum Cp value until Y/D between 5–10, except for $Fr_{pool} = 0.98$ (V = 5.0 m/s). This maximum of Cp with respect to Y/D is "shifting to the right" when increasing velocity, as can be more easily seen with blue dots on Figure 5.

(c) **Comparison of mean dynamic pressure with the literature for r/D = 0.00**: From point (a) and (b), the results show a certain discrepancy when compared with the previous authors' results at stagnation. Although this discrepancy could be explained with some different flow conditions, facility geometry, type of measurements, choice of how to compute the kinetic energy correction factor ϕ, the main idea regarding this difference is related to the core persistence Y_c, and thus to the definition of shallow and deep pools. Most previous researchers found a core jet impact for pool depth ratios up to 4.0–7.5 Y/D. In the present study, the authors measured high values of stagnation pressures, typical of the impact of the jet core for various jet velocity values. The most relevant difference with the previous authors is the persistence of the jet core impact up to 9.7 Y/D, for velocities V of 14.7 and 18.0 m/s (cf. Table 3). This long persistence of jet centreline velocities, with little velocity decay in depth, leading to high stagnation pressures at impact, reflects the stable and

compact character of the jets generated at LNEC's facility and the lower disturbance provided by pool flow features as compared to other similar facilities that were explored in the past [2–5,12–15,17].

By analyzing Cp on sensors at r/D = 0.00–0.25–0.35–0.69 (cf. Figures 4 and 5), it can be mentioned that:

(a) **The influence of velocity inside the jet diameter footprint ($r/D < 0.5$)**: Increasing velocity shows a "shifting to the right" for the maximum mean dynamic pressure at distance r/D = 0.00–0.25–0.35. The study of the stagnation zone (r/D = 0.00–0.35–0.69–1.04) was made in Duarte et al. [27], concentrating on the influence of air entrainment and pressure inside fissures. The influence of these velocities on the results was already observed in this research but was not explored in terms of the Cp coefficient with different velocities and pool depths along the flat bottom, which makes it difficult to compare the results.

(b) **Pressure evolution inside the jet diameter footprint ($r/D < 0.5$)**: $\frac{Cp_{r/D}}{Cp_0}$, the pressure ratio between $Cp_{r/D}$, at a radial distance r/D, and Cp_0, at the jet centreline $r/D = 0.00$, respectively, for each pool depth considered Y, shows an important decrease in mean dynamic pressure, moving away from the jet centreline, even inside the jet diameter footprint ($r/D < 0.5$). Table 4 summarizes results of this ratio, representing the remaining pressure at a distance of r. For example, at $r/D = 0.35$, the average of the ratios $\frac{Cp_{r/D=0.35}}{Cp_0}$ is 72% for shallow pools and 79% for deep pools.

(c) **Pressure outside the jet diameter footprint ($r/D = 0.69$)**: Differing from previous observations made inside the jet diameter footprint, no increase in Cp values was found while increasing Y/D for $r/D = 0.69$. This is nearly constant with the pool depth, with a smooth decrease. In addition, at $r/D = 0.69$, the average of the ratios $\frac{Cp_{r/D=0.69}}{Cp_0}$ drops to 41% for shallow pools and 44% for deep pools.

Table 4. Summarizing results of the radial mean dynamic pressure ratio $\frac{Cp_{r/D}}{Cp_0}$ [%].

r/D	Min	Max	Average for Shallow Pools	Average for Deep Pools
0.25	49%	96%	82%	76%
0.35	62%	93%	72%	79%
0.69	28%	67%	41%	44%

In Figure 6, another way to show the radial study of mean dynamic pressures is presented in terms of the ratio r/Y, radial distance from jet centreline r to the pool depth Y. Ervine et al. 1997 [15] revealed a general expression for the ratio $\frac{Cp_{r/D}}{Cp_0}$ of the form $e^{-K(r/Y)^2}$, where the parameter K ranged from 30 for shallow pool depths to 50 for greater pool depths. In their study, shallow pool depths corresponded to $Y/D < 4$. Duarte et al. 2015 [27], by studying a jet velocity of $V = 22.1$ m/s, found that parameter K varies roughly between 25 for $Y/D = 4.2$ and 250 for $Y/D = 11.1$. Bollaert 2002 [2] matched Ervine et al. 1997 [15] curve for deep pools using $Y/D = 8.3$ but not for shallow pools using $Y/D = 2.7$. In Figure 6, new data of this study, considering different core lengths Y_c following velocities according to Table 3, showed regressions with parameters K ranging from 75 for shallow pool depths and 157 for greater pool depths. The higher value of K for shallow pools could be explained by the fact that, in this experiment, not very shallow pools were considered since the minimum ratio available Y/D is 4.2.

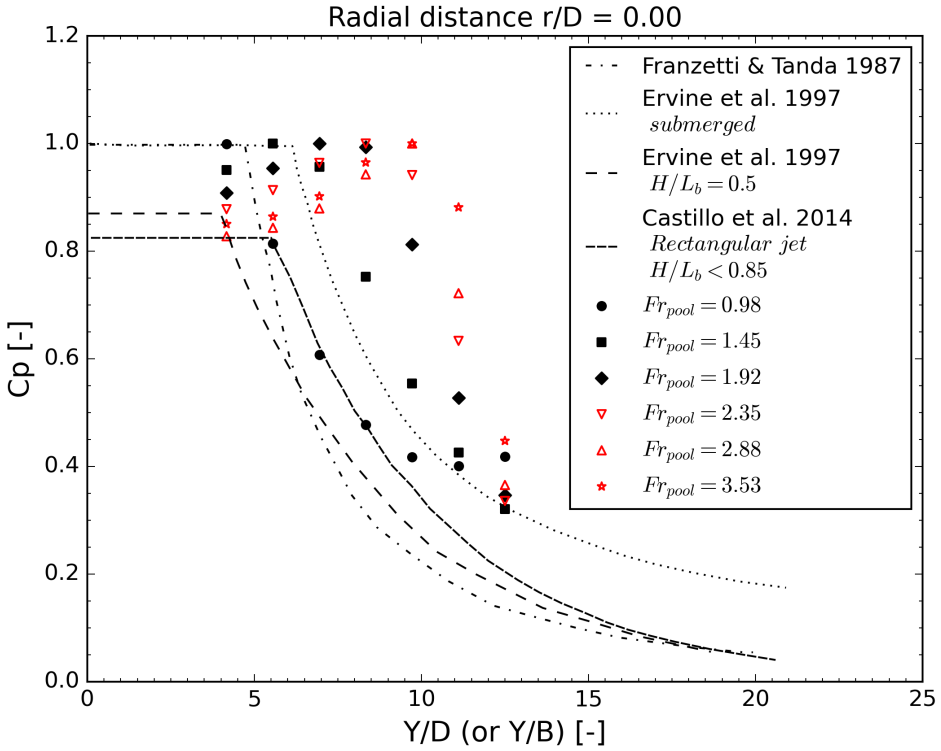

Figure 4. Mean dynamic pressure coefficient Cp [-] as a function of the pool depth ratio Y/D—at a radial distance $r/D = 0.00$—Jet break-up length ratio $H/L_b \leq 0.68$.

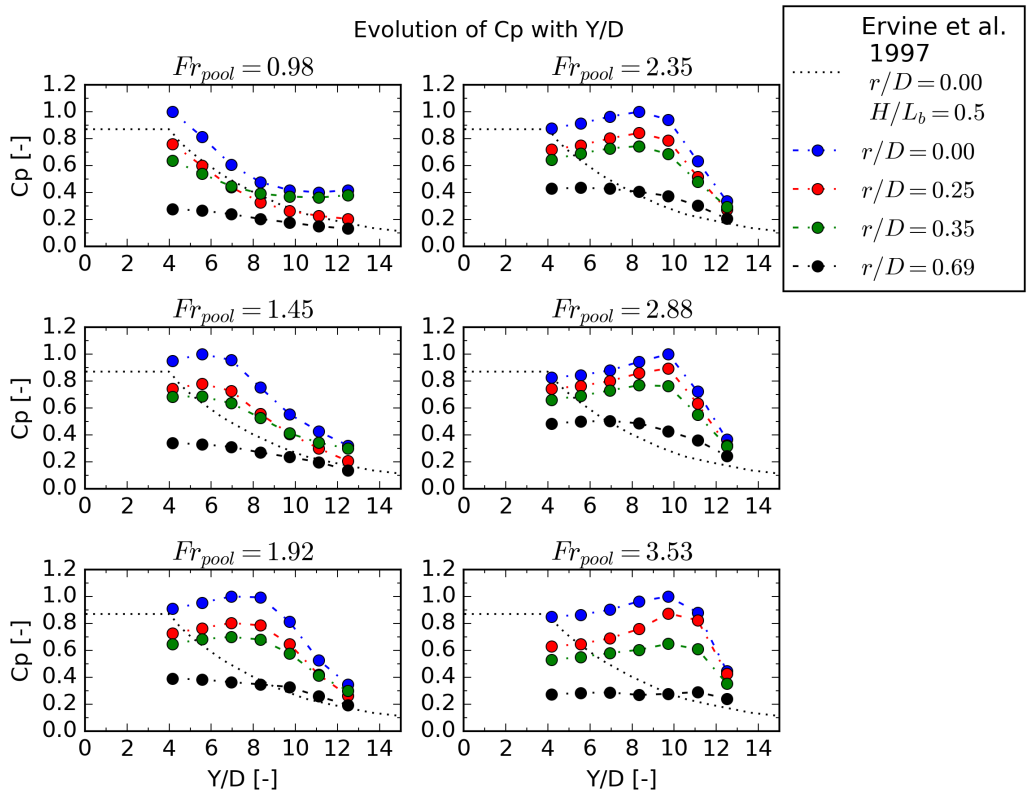

Figure 5. Mean dynamic pressure coefficient Cp [-] as a function of the pool depth ratio Y/D—at a radial distance r/D = 0.00–0.25–0.35–0.69—Jet break-up length ratio $H/L_b \leq 0.68$.

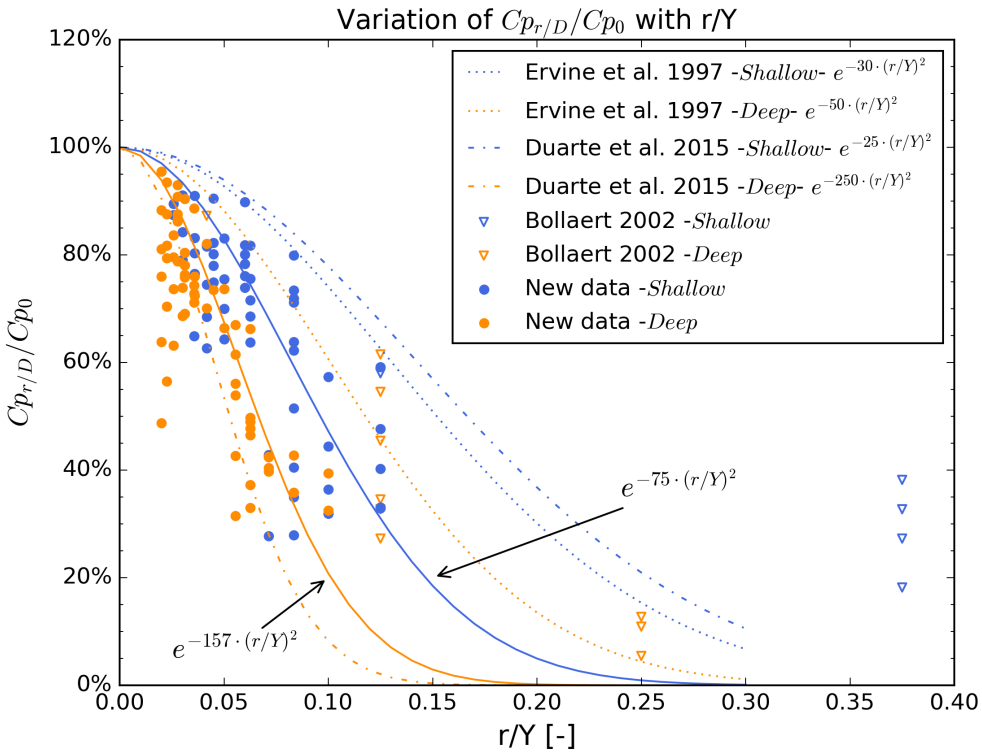

Figure 6. Variation of $\frac{Cp_{r/D}}{Cp_0}$ with r/Y out from jet centreline—difference made between shallow and deep pools.

3.2. Radial Study of Fluctuating Dynamic Pressures — $0.00 \leq r/D \leq 0.69$

The fluctuating dynamic pressure coefficient Cp', as defined in Equation (4), is strongly influenced by the initial turbulence intensity Tu; thus, the ratio H/L_b, and the aeration of the jet (cf. Tables 1 and 2 for test parameters). For this fluctuating parameter, a wide range of curves' trend interpolated by other authors was noted. In literature study, it is not clear if a proper formula for Cp' exists. Therefore, to simply illustrate and compare our data, four authors' best fits were added to the Figure 7. For more author comparisons, see Bollaert and Schleiss [19]; Castillo et al. [17]. The authors uniformly agreed that increasing the pool depth Y/D can have a counter-productive effect on fluctuations because the jet diffuses more, creating a turbulent flow in the pool, and promoting fluctuations in its bottom vicinity.

By analyzing Cp' data on sensors at r/D = 0.00–0.25–0.35–0.69 (cf. Figures 7 and 8), it can be mentioned:

(a) **Influence of acquisition frequency on measured pressure fluctuations**: It should be said that higher values of fluctuating pressures Cp' were measured using a frequency acquisition of 2400 Hz compared to values measured using 600 Hz. This was especially observed for higher velocities (V = 12.0–14.7–18.0 m/s) and shallow pool depths (Y/D < 6–8), where higher values of Cp' were noticed for 2400 Hz of about 10–30%. Comparing power spectra from 600 Hz and the ones with 2400 Hz showed a similar loss of information concerning turbulence with high frequencies and a low energy content. The sensor outside the jet diameter footprint was more subjected to differences in Cp'. This observation could bring to the unsafe side of engineering practice if too low acquisition frequency is used. This is why only the results of fluctuations recorded at 2400 Hz are presented.

(b) **Comparison of fluctuations with the literature for *r/D* = 0.00**: A good envelope was found for Cp' data from the plot of Bollaert [2]. The closest sensor to the jet centreline in Bollaert's work was at $r/D = 0.35$ but, following the results in Figure

8, it is still relevant to plot values of sensors at different radial distance r/D on the same graph. Indeed, distance from the jet axis has a far lesser influence on pressure fluctuations Cp' compared to the influence on Cp when looking at sensors of up to $r/D \leq 0.5$, i.e., those still inside the jet diameter's footprint. Regarding other author contributions, (Bollaert & Schleiss [19]; Castillo et al. [17]), one can observe the wide range of trends observed when best fitting their data to the evaluation of the fluctuations. A peak in fluctuations was obtained in nearly all previous studies around a pool depth of Y/D = 4–6. However, as can be seen in Figure 8, this is not what was observed in the present study.

(c) **Maximum value of fluctuations with respect to *Y/D***: In Ervine et al. 1997 [15], the maximum is around $Cp' = 0.2$ for $Y/D = 6$. Globally, a concentration of values is detected around this point, but the same maximum peak for $Y/D = 6$ cannot be clearly observed. In the dataset at our disposal, maximum values of Cp appear between Y/D = 6 and 11. As the velocity V increases (Fr_{pool}), the maximum value of Cp' is " shifting to the right ", meaning that increasing the pool depth ratio Y/D can have a counter-productive effect on the pressure fluctuations acting on the pool bottom. A similar phenomenon was already observed for Cp, and is more visible for Cp' in the Figure 8 with fewer data plotted in one graph. More tests should be performed to obtain a more relevant statistical study, over a wider range of velocities, to observe if this "shift to the right" is confirmed and progresses with velocities higher than $V = 18$ m/s.

3.3. Power of the Jet in the Frequency Domain—$0.00 \leq r/D \leq 0.69$

The following use of a power spectral density study aims to characterize the frequency composition of the energy content, i.e., the variance σ^2 representing the fluctuations. As non-dimensional spectra $P_{xx}/Variance$ [Hz^{-1}] are plotted herein, there is no pretension at evaluating the power of each frequency phenomenon that dimensional spectra can allow. The area under the curve of a non-dimensional spectrum is equal to 1, since the integral of a power spectral density in [$Unit^2/Hz^{-1}$] is equal to the variance σ^2 of the studied signal. In other words, large-scale eddies of the pool flow correspond to the lowest frequencies and small-scale eddies correspond to higher frequencies. For the power spectral study, use was made of Welch's method under the Python Numpy Package; 2^{19} = 524,288 values were recorded with an acquisition frequency of 2400 Hz; 128 blocks of 8192 values each considering an overlapping of 50%; use of the "Hamming" window. Graphs replacing the frequency f with Strouhal non-dimensional number $St = f \cdot D/V$ involving time, length and velocity are not presented. In Figure 9, three parameters will be studied:

- **Pool depth**: shallow pool ($Y/D = 4.2$) and deep pool ($Y/D = 12.5$).
- **Radial distance from jet axis**: inside the jet diameter footprint ($r/D < 0.50$) and outside ($r/D > 0.50$).
- **Velocity of the jet**: influence of velocity V on distribution of spectral content (from V = 5.0 m/s to 18.0 m/s).

The Figure 9 provides a range of interesting information, which is analyzed in the following four points:

(a) Differences in variance distribution inside ($r/D < 0.50$) and outside the jet diameter footprint ($r/D > 0.50$). Inside, the three considered sensors (r/D = 0.00–0.25–0.35) follow the exact same trends, as opposed to the sensor outside at $r/D = 0.69$ (comparing colored spectra and grey/black spectra on the Figure).

(b) Differences in variance distribution for shallow and deep pool depths; thus, the impact of a predominantly core jet against a more developed one. As the pool depth increases, a reduction in the high frequencies' participation in the spectrum is observed. At a deep pool depth ($Y/D = 12.5$), most energy is dissipated on low frequencies with a high amplitude, represented by large eddies of turbulent flow recirculating due to the deflection and limited size of the facility;

(c) Similarly to the trend observed in Cp, Cp', the "shift to the right" with increasing velocity is noticed with the small concave shape formed in the spectra. This break-point of the decay is the starting frequency of the dissipation zone, which leads to the cascade of energy, distributing the energy from large-scale eddies to small ones with higher frequencies. Thus, by increasing the velocity of the jet, more energy is shifted to high-frequency phenomena. This transition point, influenced by velocity, moves from approximately 15 Hz (V = 5.0 m/s) to 100 Hz (V = 18.0 m/s) for the shallow pool and from 3 Hz (V = 5.0 m/s) to 25 Hz (V = 18.0 m/s) for the deep pool. The influence of velocity on the spectral distribution was also observed in Manso et al. [28], studying laterally confined plunge pools.

(d) Following previous researches and confirmed by EPFL researchers [19,21,27,28], there is a predominance of linear slope decay of f^{-1} for shallow pools, even at high frequencies, and a sudden decay of $f^{-5/3}$ or $f^{-7/3}$ for deep pools. In Figure 9, the latter observation on the predominance of slopes for deep pools can be validated, but no linear decay with slope f^{-1} is perceived at high frequencies, meaning that the minimum depth Y/D = 4.2 available likely does not represent a shallow pool depth with core impact conditions. Moreover, EPFL experiments were recorded at 1000 Hz, 2.4 times less than on the graphs presented here, and it was shown that, in some cases, information can be lost if a sufficiently high acquisition frequency is not used. This is why, to the authors' knowledge, no such slope of $f^{-20/3}$ was already observed on the highest range of frequencies ($f > 500$ Hz).

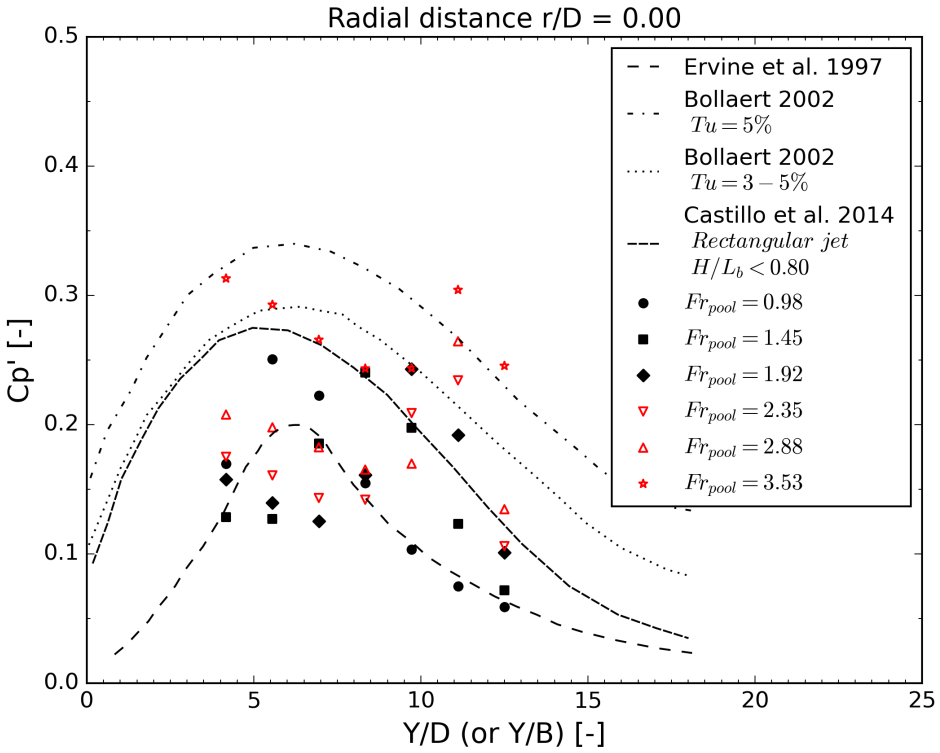

Figure 7. Fluctuating dynamic coefficient Cp' [-] as a function of the pool depth ratio Y/D—at a radial distance $r/D = 0.00$—Jet break-up length ratio $H/L_b \leq 0.68$.

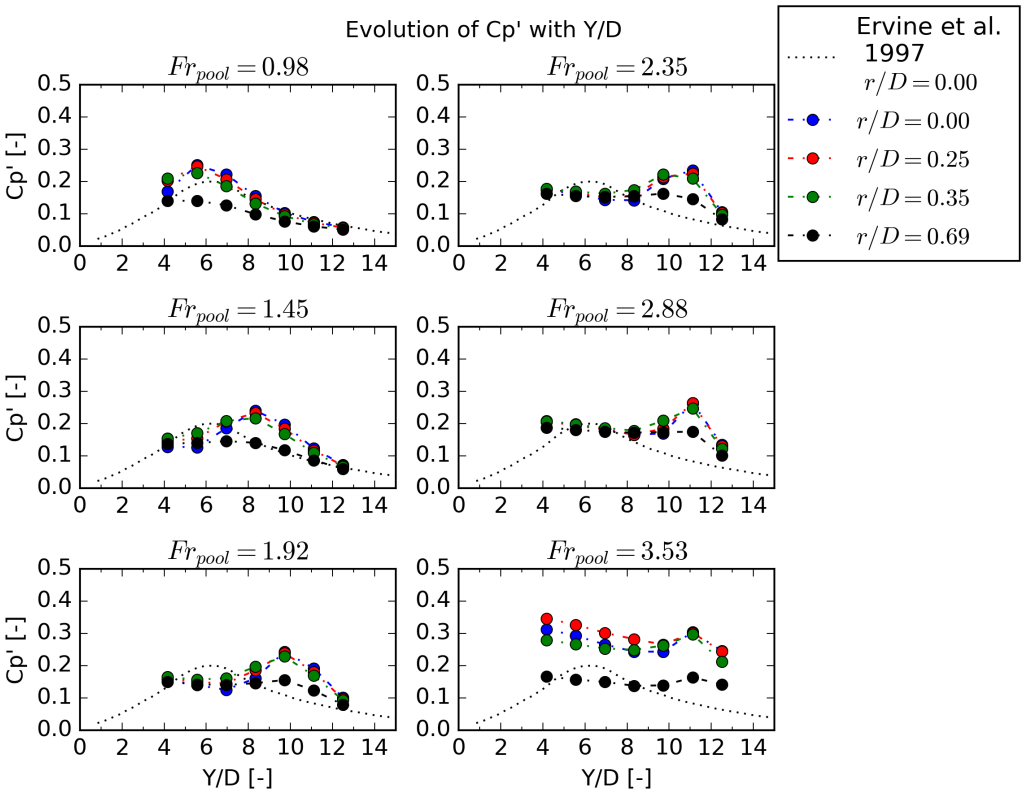

Figure 8. Fluctuating dynamic coefficient Cp' [-] as a function of the pool depth ratio Y/D—at a radial distance r/D = 0.00–0.25–0.35–0.69—Jet break-up length ratio $H/L_b \leq 0.68$.

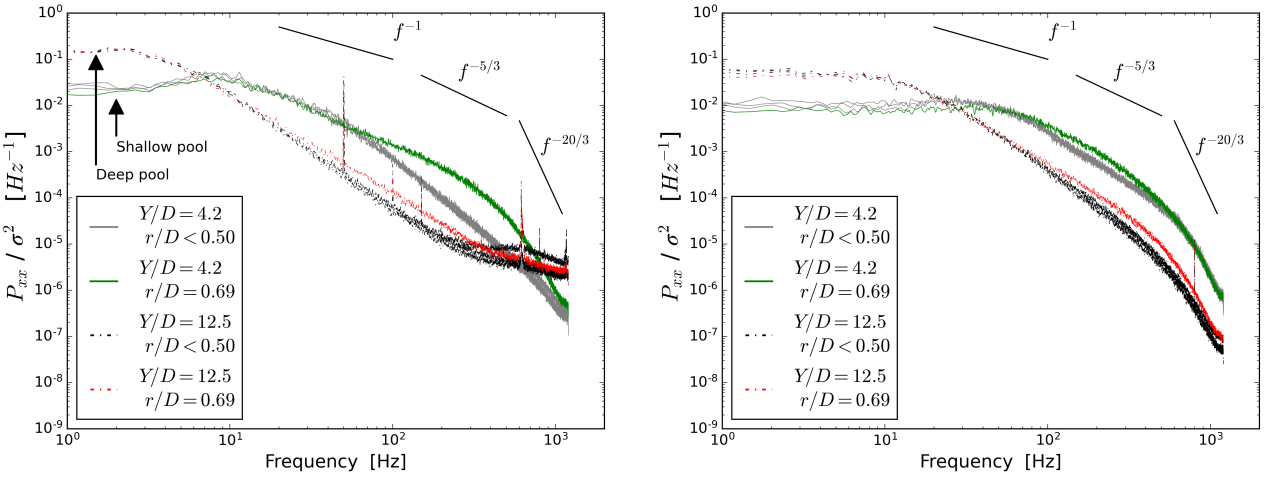

(**a**) (**d**)

Figure 9. *Cont.*

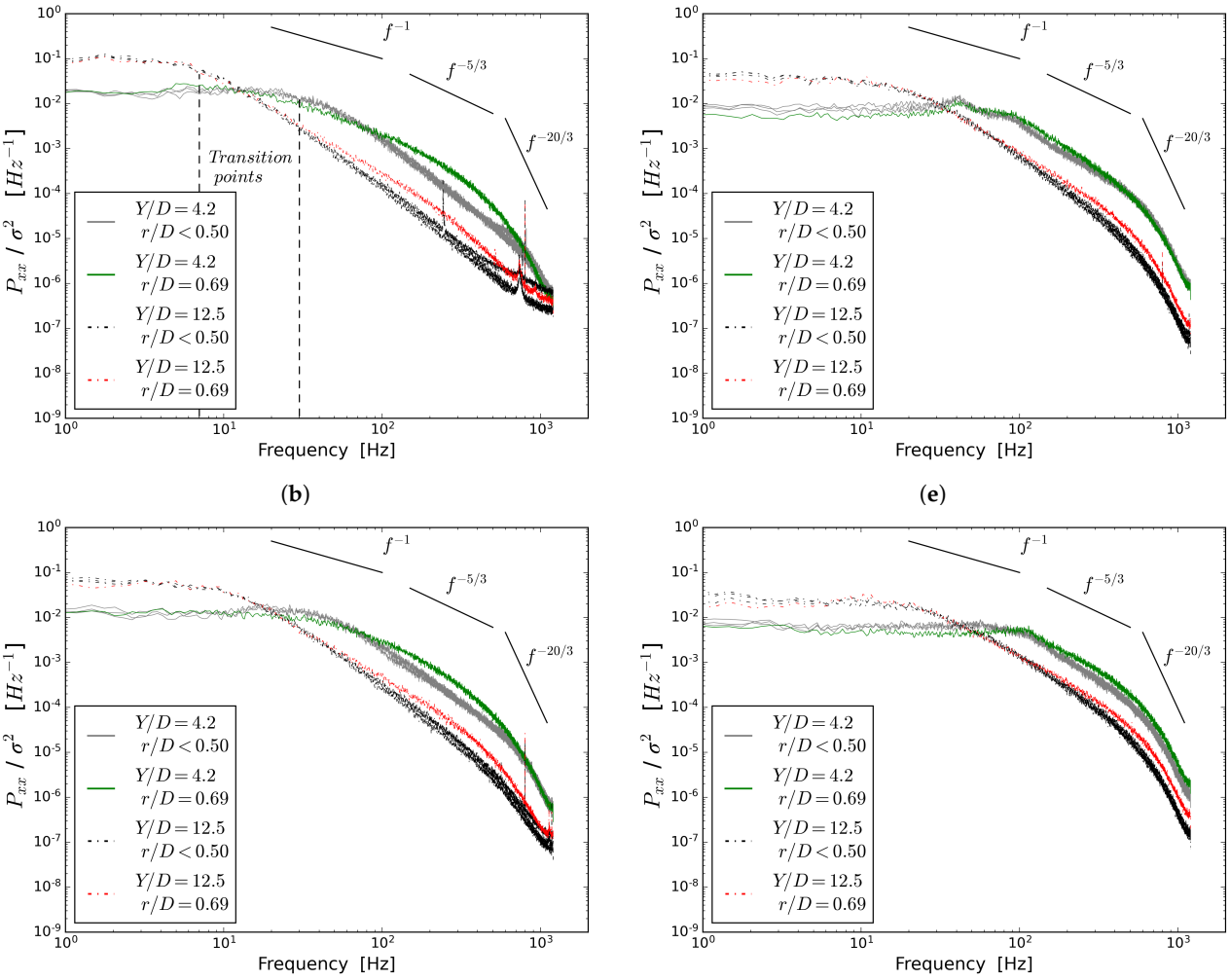

Figure 9. Evaluation of influence of Y/D (shallow/deep pool), radial distance r/D and velocity V on non-dimensional spectral content P_{xx}/σ^2 [Hz^{-1}]. (**a**) V = 5.0 m/s; (**b**) V = 7.4 m/s; (**c**) V = 9.8 m/s; (**d**) V = 12.0 m/s; (**e**) V = 14.7 m/s; (**f**) V = 18.0 m/s.

4. Conclusions

Impact pressures of plunging jets were investigated with velocities ranging from 5 to 18 m/s under an acquisition frequency of 2400 Hz. Results from the 2400 Hz tests are analyzed in the present paper, due to loss of information on energy content spectra recorded at 600 Hz. This was confirmed by the systematically higher values of fluctuations Cp' observed with 2400 Hz compared to 600 Hz, which intensifies with higher velocities ($V > 12$ m/s) and shallow pool depths ($Y/D < 6$–8).

Special attention was paid to the dynamic pressures in the plunge pool floor in the vicinity of the jet stagnation zone. This refined approach allows future research to observe the difference between the area inside and outside the jet diameter footprint, mainly in terms of mean dynamic coefficient, which is strongly influenced by a small variation in distance. The spectral content also showed a difference in the variance distribution (cf. Table 4; Figures 6 and 9).

The study shows the influence of the velocity in the obtained results. This phenomenon can possibly be explained by the recirculating currents in the plunge pool, whose intensity increases with jet velocity, and are an inevitable consequence of the fixed and limited size of the experimental facility. Aeration in the pool reduces shear stress, and thus reduces the dissipation of the jet. These two complementary processes could explain the differences found in Cp and Cp' versus Y/D if compared with the literature; for example, in Bollaert

& Schleiss [19]; Castillo et al. [17]. This observation led to the consideration of a Froude number Fr_{pool}, relating the velocity of the jet to a dimension of the pool. The research performed at EPFL, for example, defined their jets as "high-velocity" up to 32 m/s on a 3 m diameter circular plunge pool. In the present study, velocity ranged from 5 to 18 m/s in a 2.65×4 m^2 rectangular facility. These aspects, concerning the potential influence of velocity, due to the fixed and limited dimensions of the pool, deserve further investigation to achieve a better understanding and more complete characterization, e.g., by studying different size plunge pool facilities and higher velocities than 18 m/s (cf. Table 3; Figures 3, 5 and 8).

Author Contributions: Conceptualization, G.J., A.M., J.F.M. and P.A.M.; methodology, A.M. and J.F.M.; software, G.J. and A.M.; validation, G.J., A.M., J.F.M., P.A.M. and G.D.C.; formal analysis, G.J., A.M. and J.F.M.; investigation, G.J. and A.M.; resources, G.J., A.M., J.F.M., P.A.M. and G.D.C.; data curation, G.J. and A.M.; writing—original draft preparation, G.J., A.M. and J.F.M.; writing—review and editing, G.J., A.M., J.F.M., P.A.M. and G.D.C.; visualization, G.J. and A.M.; supervision, J.F.M. and P.A.M.; project administration, J.F.M., P.A.M. and G.D.C.; funding acquisition, J.F.M. and G.D.C. All authors have read and agreed to the published version of the manuscript.

Funding: This research was co-funded by "Fundação para a Ciência e Tecnologia" (FCT), Portugal, grant number PD/BD/135593/2018, by PL-LCH of "Ecole Polytechnique Fédérale de Lausanne" (EPFL), Switzerland, and by the "Swiss-European Mobility Programme" (SEMP), Switzerland, granted by the foundation "Movetia", grant number 2020-1-CH01-KA103-0045.

Institutional Review Board Statement: Not applicable.

Informed Consent Statement: Not applicable.

Data Availability Statement: All data needed to evaluate the conclusions are present in this paper, except for the data from an acquisition frequency of 600 Hz. Only data of 2400 Hz are presented herein. Additional data may be requested from the authors.

Acknowledgments: The suggestions and support by Helena M. Ramos from the Instituto Superior Técnico (IST Lisbon) and by the anonymous reviewers are acknowledged. The experimental work was performed at the LNEC, Lisbon, Portugal.

Conflicts of Interest: The authors declare no conflict of interest.

List of Symbols

r	radial horizontal distance from jet axis
D	diameter of the jet at issuance
B	thickness of the jet at impingement (rectangular case)
Y	pool depth
W_{pool}	pool width
H	jet travel distance in the air
L_b	jet break-up length in the air
Y_c	jet core persistence (core development length)
V	velocity at issuance
V_j	velocity at impact with water mattress
ϕ	correction factor for non-uniform distribution at nozzle exit: $\phi \cdot V_j$
g	gravitational acceleration; $g = 9.81$ m/s^2
σ	standard variation of a data sample
u'	root-mean-square (RMS) value of the axial component of turbulent velocity
Tu	turbulence intensity; $Tu = u'/V$
Re	Reynolds number; $Re = (V \cdot D)/\nu$
Fr	Froude number; $Fr = V/\sqrt{g \cdot D}$
Fr_{pool}	Froude pool number; $Fr_{pool} = V/\sqrt{g \cdot W_{pool}}$
ν	kinematic viscosity $\nu = 1.15 \cdot 10^{-6}$ m^2/s at 15 °C
Q	discharge
Cp	mean dynamic pressure coefficient
$Cp_{r/D}$	mean dynamic pressure coefficient at a distance r/D (can be written as Cp_r)

Cp_0	mean dynamic pressure coefficient at a distance $r/D = 0$ (stagnation point)
Cp'	fluctuating dynamic pressure coefficient
P_{mean}	mean pressure value of a data sample
S_{xx}	spectral power content [Unit^2/Hz]

References

1. ICOLD. *Technical Advancements in Spillway Design — Progress and Innovations from 1985 to 2015*; Prepared by ICOLD Technical Committee on Hydraulics for Dams, Chapter 3; ICOLD: Paris, France, 2016.
2. Bollaert, E. Influence of Transient Water Pressures in Joints on the Formation of Rock Scour Due to High-Velocity Jet Impact. Ph.D. Dissertation, École Polytechnique Fédérale de Lausanne (EPFL), Lausanne, Switzerland, 2002.
3. Manso, P.F.A. The influence of Pool Geometry and Induced Flow Patterns in Rock Scour by High-Velocity Plunging Jets. Ph.D. Dissertation, École Polytechnique Fédérale de Lausanne (EPFL), Lausanne, Switzerland, 2006
4. Federspiel, M. Response of an Embedded Block Impacted by High-Velocity Jets. Ph.D. Dissertation, École Polytechnique Fédérale de Lausanne (EPFL), Lausanne, Switzerland, 2011.
5. Duarte, R. Influence of Air Entrainment on Rock Scour Development and Block Stability in Plunge Pools. Ph.D. Dissertation, École Polytechnique Fédérale de Lausanne (EPFL), Lausanne, Switzerland, 2014.
6. Chanson, H.; Aoki, S.; Hoque, A. Physical modelling and similitude of air bubble entrainment at vertical circular plunging jets. *Chem. Eng. Sci.* **2004**, *59*, 747–758.
7. Chanson, H. Velocity mesurements within high velocity air-water jets. *J. Hydraul. Res.* **1993**, *31*, 365–382.
8. Toombes, L.; Chanson, H. Free-surface aeration and momentum exchange at a bottom outlet. *J. Hydraul. Res.* **2007**, *45*, 100–110.
9. Pfister, M.; Schwindt, S. Air concentration distribution in deflector jets. In Proceedings of the 5th IAHR International Symposium on Hydraulic Structures, Brisbane, Australia, 25–27 June 2014.
10. Carrillo, J.M.; Ortega, P.R.; Castillo, L.G.; García, J.T. Air-water properties in rectangular free-falling jets. *Water* **2021**, *13*, 1593.
11. Guyot, G.; Cartellier, A.; Matas, J. Experimental study of air entrainment by large scale plunging jets. In Proceedings of the 10th International Conference on Multiphase Flow, ICMF, Rio de Janeiro, Brazil, 19–24 May 2019.
12. Ervine, D.A.; Falvey, H.T. Behaviour of Turbulent Water Jets in the Atmosphere and in Plunge Pools. *Proc. Inst. Civ. Eng.* **1987**, *83*, 295–314.
13. Franzetti, S.; Tanda, M.G. Analysis of turbulent pressure fluctuation caused by a circular impinging jet. In Proceedings of the International Symposium on New Technology in Model Testing in Hydraulic Research, Pune, India, 24–26 September 1987; pp. 85–91.
14. May, R.W.P.; Willoughby, I.R. *Impact Pressures in Plunge Basins to Vertical Falling Jets*; Rep. SR 242; HR Wallingford: Wallingford, UK, 1991.
15. Ervine, D.A.; Falvey, H.T.; Withers, W. Pressure fluctuations on plunge pool floors. *J. Hydraul. Res.* **1997**, *35*, 257–279.
16. Melo, J.F. Acções Hidrodinâmicas em Soleiras de Bacias de Dissipação de Energia por Jactos. Ph.D. Thesis, Instituto Superior Técnico, Lisbon, Portugal, 2001.
17. Castillo, L.G.; Carrillo, J.M.; Blázquez, A. Plunge pool dynamic pressures: A temporal analysis in the nappe flow case. *J. Hydraul. Res.* **2014**, *53*, 101–118.
18. Castillo, L.G.; Carrillo, J.M. Scour, velocities and pressures evaluations produced by spillway and outlets of dam. *Water* **2016**, *8*, 68.
19. Bollaert, E.; Schleiss, A. Affouillement du rocher par impact de jets plongeants à haute vitesse Partie I: Un résumé de l'état des connaissances. *J. Hydraul. Res.* **2003**, *41*, 451–464.
20. Manso, P.A.; Bollaert, E.F.R.; Schleiss, A.J. Impact pressures of turbulent high-velocity jets plunging in pools with flat bottom. *Exp. Fluids* **2007** *42*, 49–60.
21. Bollaert, E.; Schleiss, A. Affouillement du rocher par impact de jets plongeants à haute Partie II: Résultats expérimentaux de pressions dynamiques sur le fond fosses d'affouillement et dans des joints rocheux fermés, uni-et bidimensionelle. *J. Hydraul. Res.* **2003**, *41*, 465–480.
22. Manso, P.F.A.; Bollaert, E.F.R.; Schleiss, A.J. Evaluation of high-velocity plunging jet-issuing characteristics as a basis for plunge pool analysis. *J. Hydraul. Res.* **2008**, *46*, 147–157.
23. Chen, T.-F.; Davis, J.R. Disintegration of a turbulent water jet. *J. Hydraul. Div. ASCE* **1964**, *90*, 175–206.
24. Ervine, D.A.; McKeogh, E.; Elsawy, E.M. Effect of turbulence intensity on the rate of air entrainment by plunging water jets. *Proc. Inst. Civ. Eng.* **1980**, *69*, 425–445.
25. Melo, J.F. Reduction of plunge pool floor dynamic pressure due to jet air entrainment. In *Rock Scour Due to Falling High-Velocity Jets*; Schleiss, A., Bollaert, E., Eds.; Swets and Zeitlinger: Lisse, The Netherlands, 2002; pp. 125–136.
26. Manso, P.F.A.; Bollaert, E.F.R.; Schleiss, A. Influence of Plunge Pool Geometry on High-Velocity Jet Impact Pressures and Pressure Propagation inside Fissured Rock Media. *J. Hydraul. Eng.* **2009**, *135*, 10.

27. Duarte, R.; Schleiss, A.J.; Pinheiro, A. Influence of jet aeration on pressures around a block embedded in a plunge pool bottom. *Environ. Fluid Mech.* **2015**, *15*, 673–693.
28. Manso, P.; Schleiss, A.; Boillat, J.L.; Bollaert, E. Large-scale motion induced by turbulent plunging jets in pools created by scouring of the riverbed. In *River Flow 2006: Proceedings of the International Conference on Fluvial Hydraulics, Lisbon, Portugal, 6–8 September 2006*, 1st ed.; CRC Press: Boca Raton, FL, USA, 2006; pp. 657–666.